Check for updates

Modeling Squeeze Films in the Vicinity of High Inertia Oscillating Microstructures

Nadim A. Diab[1]
Department of Mechanical Engineering,
American University of Beirut,
Beirut 1107 2020, Lebanon
e-mail: nad07@mail.aub.edu

Issam Lakkis
Department of Mechanical Engineering,
American University of Beirut,
Beirut 1107 2020, Lebanon
e-mail: issam.lakkis@mail.aub.edu

This work investigates the effect of various assumptions proposed by the classical Reynolds lubrication equation. In particular, a microplate oscillating at high frequencies (beyond cutoff) and high velocities leading to appreciable displacement within the film gap is studied. An analytical model is derived with special emphasis on the fluid's inertia effect on the fluid/solid interface. By implementing the direct simulation Monte Carlo (DSMC) method, a numerical method for modeling rarefied gas flow, the analytically based model is adjusted for the force exerted by the gas on the oscillating microstructure to capture various significant effects related to the fluid's inertia, compressibility, stiffness, and damping. [DOI: 10.1115/1.4026588]

Downloaded from http://asmedigitalcollection.asme.org/tribology/article-pdf/136/2/021705/6284892/trib_136_02_021705.pdf by American University of Beirut Aub user on 20 March 2024

1 Introduction

With the development of microelectromechanical system (MEMS) technology, many different techniques have been used to study and design microsystems for various applications, including microresonators and vibrating structures such as radio frequency (RF) MEMS. To better understand the behavior of RF MEMS, many models have been suggested in the literature to describe the physical behavior of the gas (usually air) film between the vibrating plate or beam and the fixed substrate underneath. With the emerging micro- technology in the early 90s, many researchers have reflected back on the Reynolds lubrication equation [1], due to the interest in fluid film behavior in bearings. Andrews et al. [2] and Zook et al. [3] conducted experiments to study the accuracy of the model in Ref. [1] at different frequency ranges and plate-structure spacings and to measure the quality factor of a vibrating double-clamped beam microsensor. Extensive analytical and experimental work has been done to propose different models for air damping coefficients [4] with different boundary conditions [5,6], operating ambient pressure [7,8], microplate motion [9,10],, operating frequency range [11,12], and microplate geometries [13]. Li et al. [14] and Nayfeh et al. [15] included the effects of the electrostatic driving force (actuation voltage) on the deflection of the oscillating microbeams of different shapes (fixed-fixed and fixed-free). Sumali [16] and Mol et al. [17] conducted experiments based on the frequency and time domain analyses, respectively, to model the gas squeeze film damping behavior. Zhang and Fang [18] analyzed the capacitance of an electrostatically actuated RF MEMS capacitor. The authors' main contribution was in dividing the gap between the substrate and moving plate into two different regions: the parallel (nonbended) part of the plate and the deflected part, which presents a better model due to the existence of a nonlinear electrostatic actuation force in these devices. Niessner et al. [19] discretized the nonlinear compressible Reynolds equation and modeled the gas damping coefficients as different resistors at the plate boundaries, plate holes, and air film in between the moving and fixed plates. Sumali et al. [20] studied the air drag force (free space damping) on a vibrating microcantilever beam that is away from any fixed substrate. They conducted experiments to compare the gas damping coefficients with the models of the literature (see, for example, Refs. [4,5,8]) and verified that Ref. [8] was the most accurate in the free molecular and viscous regimes. Hosaka et al. [21] modeled the behavior of microcantilever beams by including the squeeze film damping effects for the beam side facing the fixed substrate, free space damping effects on the beam face not facing the fixed substrate, internal structural damping, and the support loss at the microbeam's base. They concluded that the squeeze and free space damping dominates the structural and support loss damping effects for small cantilever beams. As the beam's length increases, the structural and support loss damping effects are unchanged while the squeeze damping decreases at a higher rate than the free space damping. It is worth noting that the free space force was modeled based on a series of assumptions from Kokubun's bead model [22]. Veijola [23] extended the Reynolds squeezed film damping equation model by introducing the gas rarefaction effects and inertia effects and used reduced order modeling (circuit analysis) to solve the resulting improved equations. Gallis and Torczynski [24] modified the Reynolds equation model for squeezed film damping by correcting for the pressure boundary conditions at the beam tips compared to the previously used trivial ambient pressure conditions. They used the Navier–Stokes slip-jump and the DSMC methods to determine the new pressure boundary condition coefficients. Lee et al. [25] extended the work of Refs. [23,24] by accounting for the higher order bending modes in deriving a new squeezed film damping ratio model. Such an extension provided an improved model that gave better results as compared to the experimental data carried out by the authors themselves since it accounts for the bending of the beam structure. A main restriction in their work is that the cantilever beam deflection was restricted to two orders of magnitude smaller than the film gap height to ensure the validity of the linear damping model. Guo and Alexeenko [26] used the ellipsoidal statistical Bhatnagar–Gross–Krook model of the equilibrium distribution function in the quasi-steady Boltzmann kinetic model to derive expressions for the gas film damping coefficient and the quality factor. Their results showed the importance of the vibrating beam's structural damping as compared to the fluid damping in the vicinity of a high Kn number (free molecular regime). However, their work was simplified by assuming a small vibration amplitude as compared to the film gap width and the cantilever beam length to be much larger than its width, transforming their problem into a two-dimensional flow along the beam's width.

2 Problem Statement

The scope of this work is to use analytical methods to help model the behavior of the gas film between a vibrating microplate

[1]Address all correspondence to this author.

Contributed by the Tribology Division of ASME for publication in the Journal of Tribology. Manuscript received March 29, 2013; final manuscript received January 14, 2014; published online February 24, 2014. Assoc. Editor: Daniel Nélias.

 Copyright © 2014 by ASME

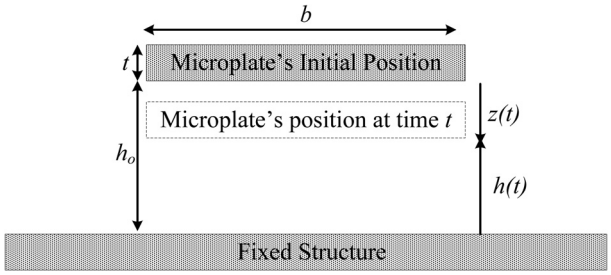

Fig. 1 Schematic of the oscillating microplate

and a fixed substrate underneath it (see Fig. 1). The microplate is allowed to move at any desired velocity amplitude and frequency such that the distance covered by the vibrating beam throughout the film gap is unlimited, where the fluid's inertia imposes a significant impact on the force exerted by the fluid on the vibrating structure. Under these conditions, the classical Reynolds lubrication equation with negligible inertia effects becomes highly unrealistic and, hence, the need for a new model that accounts for these inertia effects emerges. In what follows, a brief review on the Reynolds lubrication equation is presented, after which a new proposed model based on the analytical derivation is proposed.

3 Motivation

The DSMC simulation method summarized in the flow chart of Fig. 2 is used to compute the force of the rarefied gas on a microplate oscillating at a frequency of 1 GHz for two representative cases in Table 1, which lists a more comprehensive set of simulations. The width of the oscillating microplate (b) is 2 μm, the film gap thickness (h_0) is 1 μm, and the length of the micro-plate is $L \gg b$, resulting in a 2D problem. Readers interested in the details of applying the DSMC method to an oscillating microstructure with large displacements are referred to the authors' previous work in Refs. [27,28]. In the first case, the microplate is oscillating with a velocity amplitude (V_a) of 20 m/s where the inertia effects are expected to be negligible (Re = 1.89), while in the second case, it oscillates with a very high velocity of 400 m/s (Ma = 1.17) where the inertia effects (Re = 37.77) are expected to have a significant impact on the gas flow behavior. More importantly, Ma = 1.17 causes a wave propagation phenomenon where the microplate behaves more like a shock tube than a squeeze film. The significant effect of the gas flow inertia on the force exerted on the microplate is shown in Fig. 3, which presents the normalized force on the plate (with respect to atmospheric pressure) at different times (normalized with respect to oscillating period) within an oscillation cycle. It is clearly indicated that at the end of the first half-period ($\tau = 0.5$) when the microplate is displaced at the maximum distance from the equilibrium position and stopped, the force on the microplate's bottom face is significantly below the atmospheric pressure for the high Re case (the supersonic state), which violates the Reynolds lubrication equation. Such behavior is not encountered with the small Re case where the inertia effects are negligible. This relatively "low" pressure region is due to the fact that when the oscillating microplate reaches the bottom dead position (maximum displacement with zero velocity), the squeezed gas underneath tends to keep propagating towards the fixed substrate due to the high inertia carried by this gas flow. To better clarify this behavior, Fig. 4 shows contour plots for the gauge pressure in the vicinity of the oscillating microplate over one period. As the microplate moves towards the fixed substrate (during the first half-period where $0.1 \leq \tau \leq 0.5$), the pressure in the film gap region increases, while in the second half-period ($0.6 \leq \tau \leq 1$), as the microplate oscillates away from the fixed substrate, the pressure in the film gap region decreases. An opposite behavior is depicted on the other side of the oscillating microplate (facing the open atmosphere), as expected. The

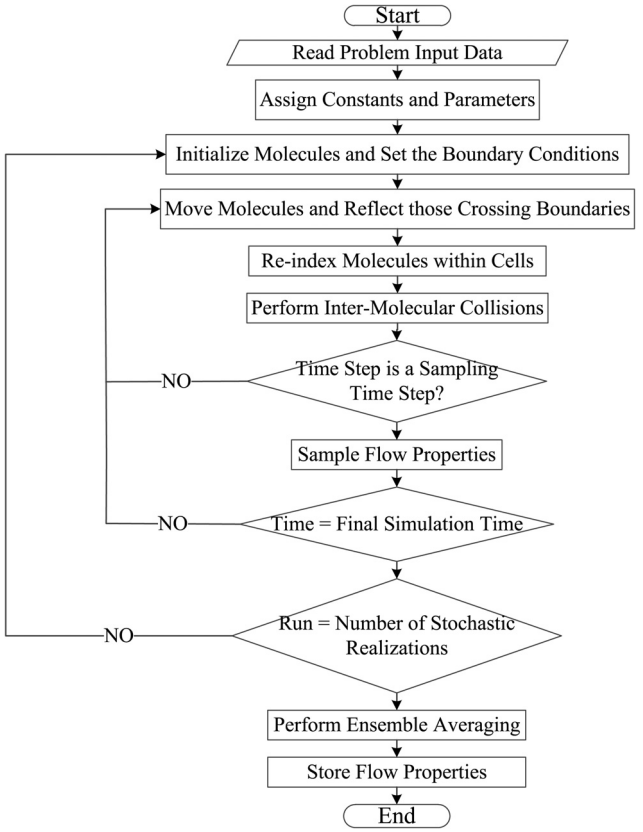

Fig. 2 Flow-chart of the DSMC algorithm

propagation of the flow is clearly shown at $\tau = 0.5$ when the microplate stops to invert its oscillating direction where a low pressure region just in front of the microplate is created due to the high flow inertia. Moreover, by looking at the pressure contours over the whole period, it is clear that the pressure at the microplate's peripheries deviates from the atmospheric pressure, as assumed by the Reynolds lubrication equation. Therefore, such phenomena stimulates the need to present a model that can better predict squeezed film damping forces where the inertia effects have a significant impact on the gas flow behavior in the vicinity of oscillating microstructures.

4 Reynolds Lubrication Equation Model

Previous work in the literature modeled the squeezed fluid film damping force based on a perturbation analysis of the Reynolds equation as derived in Refs. [1,29]. The Reynolds equation is based on the more general Navier–Stokes equation combined with the continuity equation and under the following assumptions:

(1) Newtonian fluid
(2) thin film as compared to the geometry of the squeezing structure ($h_0 \ll b$)
(3) negligible inertial effects (Re $\ll$ 1)
(4) negligible body forces

Based on the preceding assumptions, the Reynolds equation governing the fluid film behavior between two parallel plates (one fixed and the other oscillating in a rigid-nonrotating mode) is given as follows

$$\frac{\partial(ph)}{\partial t} - \frac{1}{12\mu}\left(\frac{\partial}{\partial x}\left(h^3 p \frac{\partial p}{\partial x}\right) + \frac{\partial}{\partial y}\left(h^3 p \frac{\partial p}{\partial y}\right)\right) = 0 \qquad (1)$$

where $h(t) = h_0 + \delta \sin(\omega t)$. In dimensionless form, Eq. (1) is expressed as

Downloaded from http://asmedigitalcollection.asme.org/tribology/article-pdf/136/2/021705/6284892/trib_136_02_021705.pdf by American University of Beirut Aub user on 20 March 2024

Table 1 List of dimensionless groups and model coefficients for the simulation case studies

f (MHz)	V_a (m/s)	Ma	Re	St	Error	C_1	C_2	C_3	C_4	C_5	C_6	C_7	C_8	C_9
1000	20	0.06	1.89	50	0.07	0	135.3	9.231	0	0	0	0	0	0
1000	90	0.26	8.50	11.11	0.02	0	142.4	7.864	0	0	0	0	0	0
1000	100	0.29	9.44	10	0.03	0	128.4	7.215	0	0	0	0	0	0
1000	200	0.58	18.89	5	0.06	0	112.3	5.074	0	0	0	0	0	0
1000	400	1.17	37.77	2.5	0.03	45.08	79.40	1.49	0	0	0	10.60	0	0
1000	600	1.75	56.66	1.67	0.05	90.80	66.73	−0.98	0	0	45.69	22.85	0	0
1000	800	2.33	75.54	1.25	0.09	124.01	59.77	−3.16	0	0	84.42	27.11	0	0
100	90	0.26	8.50	1.11	0.07	0	93.05	49.11	−8.87	0	0	0	−53	−13.9
500	90	0.26	8.50	5.56	0.04	0	123.3	11.99	0	0	0	0	0	0
1000	90	0.26	8.50	11.11	0.02	0	142.4	7.864	0	0	0	0	0	0
50	78.54	0.23	7.42	0.64	0.07	0	99.84	31.15	2.04	103.2	0	0	−19.1	0.26
90	141.37	0.41	13.35	0.64	0.06	0	87.99	40.96	−0.8	23.07	0	0	−40.2	−7.8
100	157.08	0.46	14.83	0.64	0.03	0	90.06	43.78	−9.05	−10.5	0	2.515	−39.9	−13.2
111.11	174.53	0.51	16.48	0.64	0.06	0	91.03	51.37	−13.6	−42.4	0	8.818	−41.1	−15.1
125	196.35	0.57	18.54	0.64	0.05	0	88.79	50.41	−9.85	−75.4	0	19.43	−34.4	−10.6
150	235.62	0.69	22.25	0.64	0.01	0	72.09	39.4	−6.6	−48.1	0	10.26	−20.5	−4.48

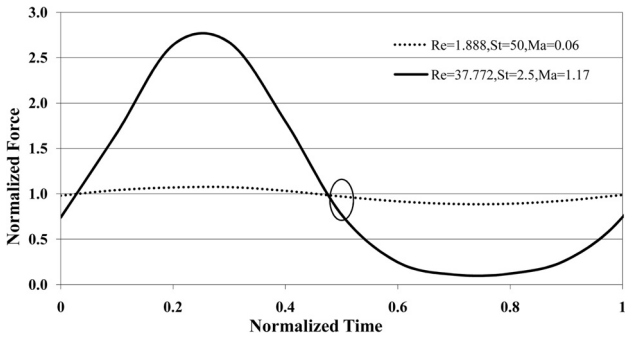

Fig. 3 Average forces on the microplate as simulated by the DSMC over one period

$$\frac{1}{\omega}\frac{\partial(PH)}{\partial t}=\frac{1}{2}\left(\frac{1}{\sigma_L}\frac{\partial}{\partial\zeta}H\frac{\partial(PH)^2}{\partial\zeta}+\frac{1}{\sigma_b}\frac{\partial}{\partial\eta}H\frac{\partial(PH)^2}{\partial\eta}\right)+\frac{1}{\sigma_L}\frac{\partial}{\partial\zeta}(PH)^2\frac{\partial H}{\partial\zeta}+\frac{1}{\sigma_b}\frac{\partial}{\partial\eta}(PH)^2\frac{\partial H}{\partial\eta} \tag{2}$$

where $\sigma_L = 12\mu L^2\omega/h_0^2P_0$ and $\sigma_b = 12\mu b^2\omega/h_0^2P_0$.

Defining the dimensionless oscillation amplitude $\varepsilon \equiv (\delta/h_0) \ll 1$ and applying the perturbation analysis where

$$PH = 1+\delta(PH), \quad \delta(PH)=\varepsilon\sin(\omega t)+\delta P \tag{3}$$

Eq. (2) is reduced to

$$\left(\frac{\partial}{\partial(\omega t)}-\left(\frac{1}{\sigma_L}\frac{\partial^2}{\partial\zeta^2}+\frac{1}{\sigma_b}\frac{\partial^2}{\partial\eta^2}\right)\right)\delta P+\varepsilon\cos(\omega t)=0 \tag{4}$$

Assuming a 2D flow ($b \ll L$) and normalizing the perturbed pressure ($\hat{p}=\delta P/P_0$)

$$\frac{\partial\hat{p}}{\partial t}=\frac{h_0^2P_0}{12\mu b^2}\frac{\partial^2\hat{p}}{\partial\zeta^2}-\frac{\dot{h}(t)}{h_0} \tag{5}$$

By further assuming that the oscillation amplitude of the moving plate is much smaller than the gap height ($\delta \ll h_0$ and, therefore, St $\gg$ 1) and the trivial boundary conditions at the plate's borders (pressure is atmospheric), the perturbation analysis is performed on the pressure change within the film gap and the force exerted by the squeezed film on the moving plate is given (in the Laplace domain) as follows [30]

$$F(s)=\left(\frac{96\mu Lb^3}{\pi^4h_0^3}\sum_{\text{nod}\,d}\frac{1}{n^4}\frac{1}{1+\dfrac{s}{\alpha_n}}\right)sz(s) \tag{6}$$

where $\alpha_n = h_0^2p_an^2\pi^2/12\mu b^2$, L is the length of the plate, and $sz(s)$ is the Laplace transform of the oscillating plate's velocity. By assuming that the microplate's oscillating frequency is much smaller than the cutoff frequency ($f \ll \omega_c$), it becomes valid to neglect the higher order terms and use the first term only of the preceding summation ($n = 1$). Then the squeezed film force can be approximated as

$$F(s)=\frac{c}{1+\dfrac{s}{\omega_c}}sz(s) \tag{7}$$

where the damping constant is $c = 96\mu Lb^3/\pi^4h_0^3$ and the cutoff frequency is $\omega_c = \alpha_1 = h_0^2p_a\pi^2/12\mu b^2$. By applying some mathematical manipulations we obtain the following expression

$$\frac{F(s)}{sz(s)}=\frac{c}{1+\dfrac{s}{\omega_c}\dfrac{c\omega_c}{s}}=\frac{c\dfrac{c\omega_c}{s}}{c+\dfrac{c\omega_c}{s}} \tag{8}$$

The preceding equation shows that the squeezed fluid force can be modeled as a parallel capacitor (representing the fluid's compressibility behavior) and resistor (representing the fluid's dissipative behavior) of the impedances $c\omega_c/s$ and c, respectively.

When the microplate is oscillating at a frequency $f \ll \omega_c$, the impedance of the capacitor becomes very large and, therefore, acts as an open circuit. In that case the fluid behaves like a damper with the dissipative effect dominating. As the frequency f increases and approaches ω_c, the compressibility of the squeezed gas film starts showing up until the point where it equals the dissipative effect. This is the point where the microplate is oscillating at the cutoff frequency ($f = \omega_c$). It is very important to note that the range of applicability of this model is restricted to frequencies up to the vicinity of the cutoff frequency, as previousl explained, where only the first term in the summation of Eq. (6) was included.

5 Flow Governing Equations

In what follows, the governing equations (continuity and momentum) will be presented in dimensionless forms using the following scales: $\rho \sim \rho_0$, $\mu \sim \mu_0$, $t \sim (1/f)$, $x \sim b$, $y \sim h_0$, $v \sim V_a$, $u \sim U$, $P \sim (\mu V_a/h_0)$, where V_a is the plate's maximum speed.

Downloaded from http://asmedigitalcollection.asme.org/tribology/article-pdf/136/2/021705/6284892/trib_136_02_021705.pdf by American University of Beirut Aub user on 20 March 2024

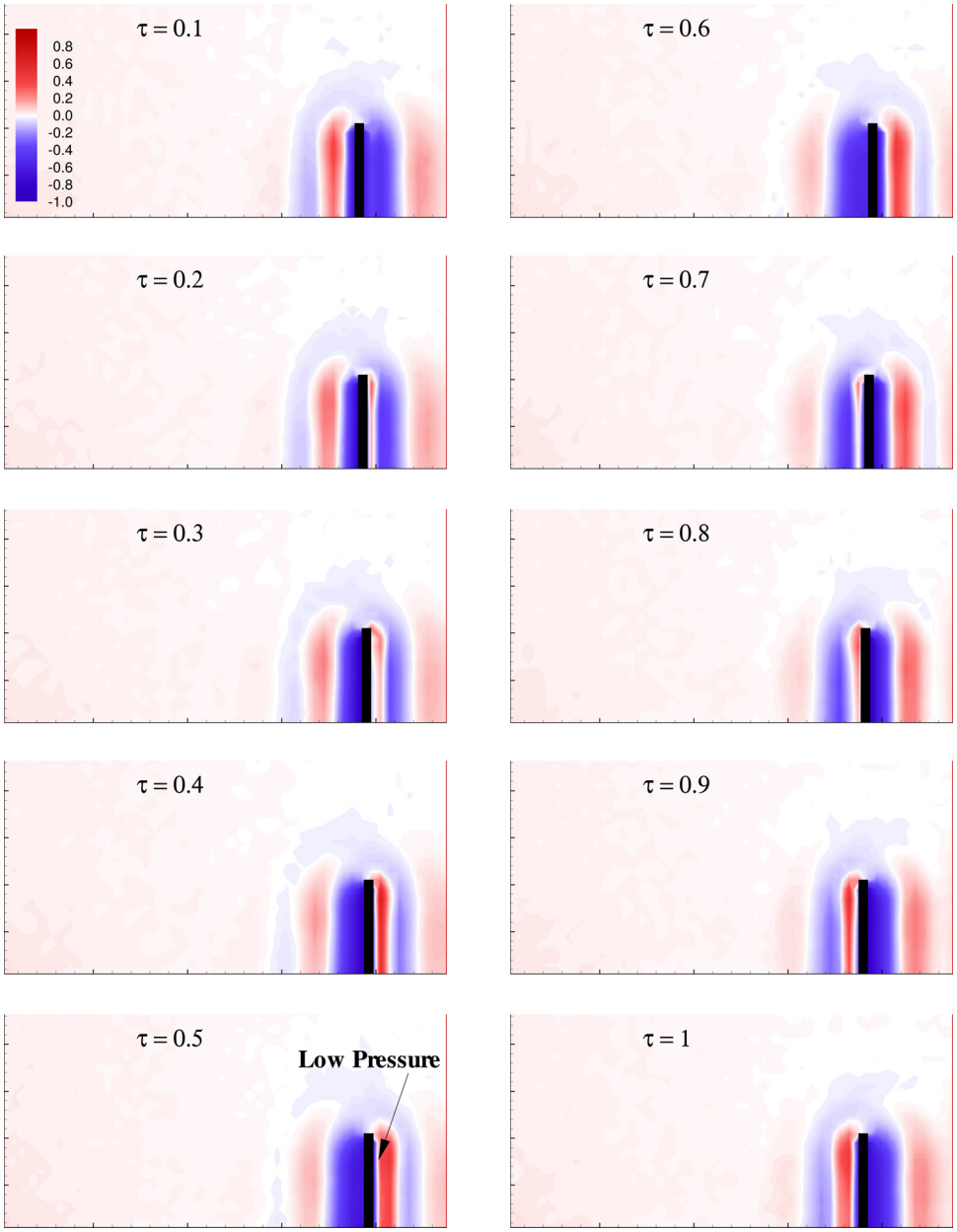

Fig. 4 Pressure profiles of the gauge pressure variation over one period in the vicinity of the microplate oscillating at 400 m/s and 1 GHz

The average horizontal flow velocity U can be found by applying the conservation of mass for the control volume in Fig. 5

$$\frac{d}{dt}(\rho h(t)dx) + \rho\frac{\partial U}{\partial x}h(t)dx = 0 \Rightarrow U(x,t) = -\int_0^x \frac{1}{h(t)}\frac{dh(t)}{dt}dx' \Rightarrow U(x,t) = -\frac{x}{h(t)}\frac{dh(t)}{dt} = -\frac{bV_a}{h_0}U^*(x,t) \quad (9)$$

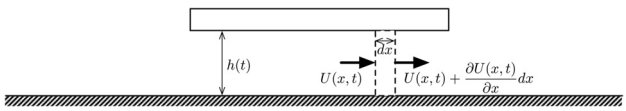

Fig. 5 Control volume 1

where

$$U(x,t) = \frac{\int_0^{h(t)} u(x,y,t)dy}{h(t)} \quad (10)$$

and, consequently, $u \sim (bV_a/h_0)$. Therefore, the first governing equation introduced is the dimensionless incompressible continuity equation given by

$$\frac{\partial u}{\partial x} + \frac{\partial v}{\partial y} = 0 \Rightarrow v(x,y,t) = \frac{y}{h(t)}\frac{dh(t)}{dt} \quad (11)$$

Applying the conservation of the $x-$momentum and multiplying both sides with h_0^3/bV_a, we obtain the second governing equation

Downloaded from http://asmedigitalcollection.asme.org/tribology/article-pdf/136/2/021705/6284892/trib_136_02_021705.pdf by American University of Beirut Aub user on 20 March 2024

$$\rho \mathrm{Re}\left(\mathrm{St}\frac{\partial u}{\partial t}+u\frac{\partial u}{\partial x}+v\frac{\partial u}{\partial y}\right)=-\left(\frac{h_0}{b}\right)^2\frac{\partial P}{\partial x}+\mu\left(\left(\frac{h_0}{b}\right)^2\frac{\partial^2 u}{\partial x^2}+\frac{\partial^2 u}{\partial y^2}\right) \tag{12}$$

where $\mathrm{Re}=\rho_0 V_a h_0/\mu_0$ and $\mathrm{St}=fh_0/V_a$.

By applying the conservation of the $y-$momentum and multiplying both sides with h_0^2/V_a, we obtain the third governing equation

$$\rho \mathrm{Re}\left(\mathrm{St}\frac{\partial v}{\partial t}+u\frac{\partial v}{\partial x}+v\frac{\partial v}{\partial y}\right)=\frac{\partial P}{\partial y}+\mu\left(\left(\frac{h_0}{b}\right)^2\frac{\partial^2 v}{\partial x^2}+\frac{\partial^2 v}{\partial y^2}\right)$$

6 Incompressible Flow Analysis

The main goal of this work is to augment the previous model by stressing the inertia effects and, therefore, we extend the Reynolds lubrication model by including the inertia of the flow as follows.

By assuming the inertial forces to be dominant over the viscous forces ($\mathrm{Re}\gg 1$), Eq. (12) becomes

$$\rho \mathrm{Re}\left(\mathrm{St}\frac{\partial u}{\partial t}+u\frac{\partial u}{\partial x}+v\frac{\partial u}{\partial y}\right)=-\left(\frac{h_0}{b}\right)^2\frac{\partial P}{\partial x} \tag{13}$$

Next we apply the conservation of the $x-$momentum for the control volume of Fig. 6

$$\rho \mathrm{ReSt}\int_x^{1/2}\frac{\partial u}{\partial t}h(t)dx+\rho \mathrm{Re}\int_x^{1/2}u\frac{\partial u}{\partial x}h(t)dx=-\left(\frac{h_0}{b}\right)^2\int_x^{1/2}\frac{\partial P}{\partial x}h(t)dx \tag{14}$$

By approximating U according to Eq. (9) and implementing the ambient atmospheric pressure conditions at the peripheries of the gap, we obtain

$$\overline{p}(x,t)-p_a=\frac{-\rho}{2}\left(\frac{b}{h_0}\right)^2\mathrm{ReSt}\left(\left(\frac{1}{2}\right)^2-x^2\right)\left(\frac{1}{h(t)}\frac{d^2h(t)}{dt^2}\right)+\rho\left(\frac{b}{h_0}\right)^2\mathrm{Re}\left(\left(\frac{1}{2}\right)^2-x^2\right)\left(\frac{1}{h(t)}\frac{dh(t)}{dt}\right)^2 \tag{15}$$

Assuming that the mean pressure $\overline{p}(x,t)$ at any distance x inside the gap is the average of the pressures at the fixed substrate ($p(x,0,t)$) and moving plate ($p(x,h(t),t)$), then Eq. (15) becomes

$$p(x,0,t)+p(x,h(t),t)=-\rho\left(\frac{b}{h_0}\right)^2\mathrm{ReSt}\left(\left(\frac{1}{2}\right)^2-x^2\right)\left(\frac{1}{h(t)}\frac{d^2h(t)}{dt^2}\right)+2\rho\left(\frac{b}{h_0}\right)^2\mathrm{Re}\left(\left(\frac{1}{2}\right)^2-x^2\right)\left(\frac{1}{h(t)}\frac{dh(t)}{dt}\right)^2+2p_a \tag{16}$$

Similarly, the inviscid dimensionless governing $y-$momentum (see Eq. (13)) becomes

$$\rho \mathrm{Re}\left(\mathrm{St}\frac{\partial v}{\partial t}+u\frac{\partial v}{\partial x}+v\frac{\partial v}{\partial y}\right)=\frac{\partial P}{\partial y} \tag{17}$$

The conservation of the $y-$momentum for the control volume of Fig. 5 is

$$(p(x,0,t)-p(x,h(t),t))dx=\mathrm{ReSt}\frac{\partial}{\partial t}\int_0^{h(t)}\rho v dx dy+\mathrm{Re}\int_0^{h(t)}\rho u(x+dx,t)v(x+dx,y,t)dy-\mathrm{Re}\int_0^{h(t)}\rho u(x,t)v(x,y,t)dy \tag{18}$$

By substituting the values of U and v from Eqs. (9) and (11) in Eq. (18) and then subtracting the resulting equation from Eq. (16), we obtain

$$p(x,h(t),t)=-\rho\left(\frac{b}{h_0}\right)^2\mathrm{ReSt}\left(\frac{1}{4}-x^2\right)\left(\frac{1}{h(t)}\frac{d^2h(t)}{dt^2}\right)+\rho\left(\frac{b}{h_0}\right)^2\mathrm{Re}\left(\frac{1}{4}-x^2\right)\left(\frac{1}{h(t)}\frac{dh(t)}{dt}\right)^2-\frac{\rho\mathrm{Re}}{4}\left(\frac{\mathrm{St}}{2}\frac{d^2h(t)}{dt^2}-\left(\frac{dh(t)}{dt}\right)^2\right)+12\mu\left(\frac{b}{h_0}\right)^2\left(\left(\frac{1}{2}\right)^2-x^2\right)\left(\frac{1}{h(t)^3}\frac{dh(t)}{dt}\right)+p_a \tag{19}$$

The average pressure at the plate's front face is given by

$$p_f=\overline{p}(h(t),t)=\frac{\int_0^{1/2}p(x,h(t),t)dx}{1/2}=\frac{-\rho}{12}\left(\frac{b}{h_0}\right)^2\mathrm{ReSt}\left(\frac{1}{h(t)}\frac{d^2h(t)}{dt^2}\right)+\frac{\rho}{12}\left(\frac{b}{h_0}\right)^2\mathrm{Re}\left(\frac{1}{h(t)}\frac{dh(t)}{dt}\right)^2-\frac{\rho\mathrm{ReSt}}{8}\left(\frac{d^2h(t)}{dt^2}\right)+\frac{\rho\mathrm{Re}}{4}\left(\frac{dh(t)}{dt}\right)^2+\mu\left(\frac{b}{h_0}\right)^2\left(\left(\frac{1}{2}\right)^2-x^2\right)\left(\frac{1}{h(t)^3}\frac{dh(t)}{dt}\right)+p_a \tag{20}$$

We now direct our attention to the flow above the plate with the control volume shown in Fig. 7, with $R\gg b$ and $R\gg h$ where ambient atmospheric pressure conditions are applied.

Applying the $y-$momentum at $x=0$ for an incompressible inviscid flow

$$\rho \mathrm{ReSt}\frac{\partial v}{\partial t}+\rho \mathrm{Re}\,v\frac{\partial v}{\partial y}=-\frac{\partial p}{\partial y} \tag{21}$$

Fig. 6 Control volume 2

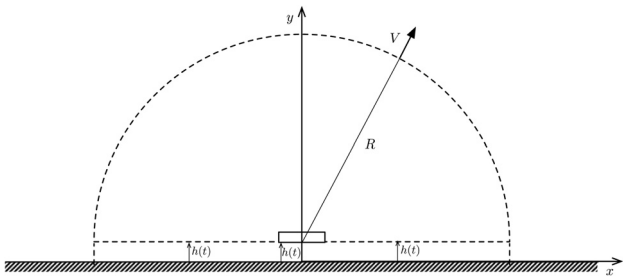

Fig. 7 Control volume 3

Downloaded from http://asmedigitalcollection.asme.org/tribology/article-pdf/136/2/021705/6284892/trib_136_02_021705.pdf by American University of Beirut Aub user on 20 March 2024

and integrating

$$\rho \mathrm{ReSt} \int_{h(t)}^{\infty} \frac{\partial v}{\partial t} dy + \rho \mathrm{Re} \int_{h(t)}^{\infty} v \frac{\partial v}{\partial y} dy = p_b - p_a \tag{22}$$

then by using the Leibniz rule to expand the first term in the preceding equation and using the values of $v(\infty) = 0$ and $v(h(t)) = dh(t)/dt$ we obtain

$$p_b = \rho \mathrm{ReSt} \frac{d}{dt} \left(\int_{h(t)}^{\infty} v dy \right) + \frac{\rho \mathrm{Re}}{2} \left(\frac{dh(t)}{dt} \right)^2 + p_a \tag{23}$$

An approximation is used where $\int_{h(t)}^{\infty} v dy \approx dh(t)/dt$, then the pressure at the plate's back face is

$$p_b = p_a + \frac{\rho \mathrm{Re}}{2} \left(\frac{dh(t)}{dt} \right)^2 + \rho \mathrm{ReSt} \frac{d^2 h(t)}{dt^2} \tag{24}$$

The net force acting on the oscillating microplate is

$$\begin{aligned} F_{\mathrm{net}} &= \int_{-1/2}^{1/2} (p_f - p_b) dx \\ &= \frac{\rho}{12} \left(\frac{b}{h_0} \right)^2 \mathrm{ReSt} \left(\frac{1}{h(t)} \frac{d^2 h(t)}{dt^2} \right) - \frac{\rho}{6} \left(\frac{b}{h_0} \right)^2 \mathrm{Re} \left(\frac{1}{h(t)} \frac{dh(t)}{dt} \right)^2 \\ &\quad - \frac{9\rho}{8} \mathrm{ReSt} \left(\frac{d^2 h(t)}{dt^2} \right) - \frac{\rho \mathrm{Re}}{4} \left(\frac{dh(t)}{dt} \right)^2 \end{aligned} \tag{25}$$

If $z(t)$ is the displacement of the microplate measured from its initial position (h_0), then the net force acting on the microplate is

$$\begin{aligned} F_{\mathrm{net}} &= -\frac{\rho}{12} \left(\frac{b}{h_0} \right)^2 \mathrm{ReSt} \left(\frac{1}{1 - z(t)} \frac{d^2 z(t)}{dt^2} \right) \\ &\quad + \frac{\rho}{6} \left(\frac{b}{h_0} \right)^2 \mathrm{Re} \left(\frac{1}{1 - z(t)} \frac{dz(t)}{dt} \right)^2 + \frac{9\rho}{8} \mathrm{ReSt} \left(\frac{d^2 z(t)}{dt^2} \right) \\ &\quad - \frac{\rho \mathrm{Re}}{4} \left(\frac{dz(t)}{dt} \right)^2 \end{aligned} \tag{26}$$

7 Fluid Force Model

In this section, the net fluid force exerted on the microplate of Fig. 1 is modeled for the simulation cases presented in Table 1, where one or more of the assumptions stated in deriving Eq. (8) are violated. The microplate is allowed to oscillate at frequencies beyond the cutoff frequency, with high speed amplitudes (inertia effects are highly significant), and moves an appreciable distance along the gap height (violating $\mathrm{St} \gg 1$). This force combines the dissipative (damping), stiffness (spring), fluid's inertia, and compressibility effects of the squeezed gas film. The numerical results obtained from the DSMC simulations are used to extend the range of applicability of the model (26) to include the inertia, damping, and compressibility effects. Therefore, a new force model with a series of higher order terms is proposed in order to minimize the error between the analytical and numerical squeezed film force as follows

$$\begin{aligned} F_{\mathrm{net}} &= C_1 z(t) + C_2 \frac{dz(t)}{dt} + C_3 \frac{d^2 z(t)}{dt^2} - C_4 \left(\frac{dz(t)}{dt} \right)^2 + C_5 z(t) \frac{dz(t)}{dt} \\ &\quad + C_6 z(t) \frac{d^2 z(t)}{dt^2} + C_7 \left(\frac{dz(t)}{dt} \right)^3 + C_8 \frac{1}{1 - z(t)} \frac{d^2 z(t)}{dt^2} \\ &\quad + C_9 \left(\frac{1}{1 - z(t)} \frac{dz(t)}{dt} \right)^2 \end{aligned} \tag{27}$$

Table 1 shows the coefficients of the various terms in the new model for different simulation case studies in addition to the L_2-norm error between the numerically evaluated force (using the DSMC) and that of the analytical model suggested in Eq. (27). These coefficients are a function of the dimensionless groups Kn, Ma, Re, and St, however, since in the presented simulations the medium gas is unchanged (constant viscosity and speed of sound) and the film gap thickness is fixed (Kn is fixed for all simulations), then Ma and Re become merely dependent (directly proportional) on the same variable (the oscillating velocity).

Figure 8 plots the dependence of the proposed force model coefficients on the dimensionless groups Re and St. The first coefficient represents the stiffness of the gas and it shows that the more the gas is compressed, the more effective the gas compressibility (or stiffness) becomes, modeled as a linear spring; therefore, this coefficient shows up for high Re and low St simulations with a stronger dependence on Re ($C_1 = f(\mathrm{Re}/\mathrm{St}^{1/4})$). The second and seventh coefficients reflect the linear and nonlinear damping components of the gas, respectively, where the linear damping element (C_2) dominates at low Re and high St ($C_2 = f(\mathrm{Re}^{1/3}/\mathrm{St}^{1/4})$). The nonlinear damping element (C_7) that is proportional to the third power of the microplate's speed gains importance at very high speeds (high Re) where the microplate displaces an appreciable distance in the gap (small St); thus, the gas becomes trapped underneath the microplate ($C_7 = f(\mathrm{Re}^{1/4}/\mathrm{St}^{1/5})$).

The third, fourth, sixth, eighth, and ninth coefficients represent the inertia of the fluid flow where the third and sixth coefficients (C_3 and C_6) reflect inertia due to the fluid's acceleration while the fourth, eighth, and ninth coefficients (C_4, C_8, and C_9) reflect inertia due to the change of mass of the squeezed fluid film. For the

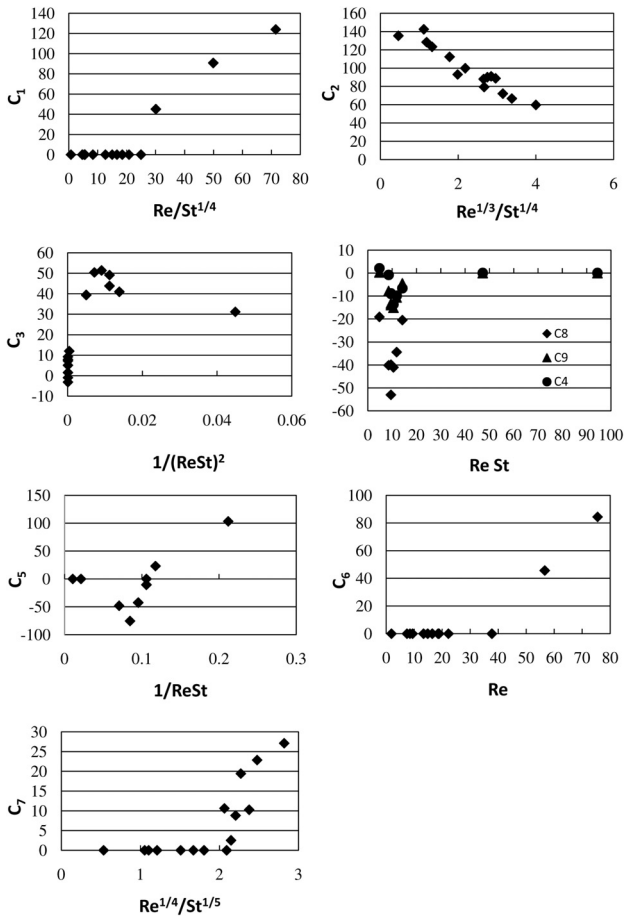

Fig. 8 Dependence of the model coefficients on the dimensionless groups Re and St

Downloaded from http://asmedigitalcollection.asme.org/tribology/article-pdf/136/2/021705/6284892/trib_136_02_021705.pdf by American University of Beirut Aub user on 20 March 2024

third coefficient, when the microplate is oscillating with high speed (high Re) at a relatively low frequency (small St), the gas in the vicinity of this structure has enough time to carry the inertia and, therefore, has a high impact on the microplate's face force ($C_3 = f(1/(\mathrm{ReSt})^2)$). Then as the frequency increases, the microplate's fast inverting motion tends to weaken any inertia effects for the surrounding gas. However, for high oscillating frequencies and as the microplate's speed also increases, some of the squeezed gas with significantly large flow velocity (supersonic flow, $\mathrm{Ma} > 1$) will be able to "escape" the inertia "destroying" effect of the microplate's fast inverting motion and, hence, causing a change in the gas inertia that is reflected by the sixth coefficient ($C_6 = f(\mathrm{Re})$). Moreover, when the microplate is oscillating at a relatively low frequency (100 MHz) along with a high speed, it gives a substantial part of the squeezed gas (during the first half-period) underneath the microplate "enough" time to escape to the surrounding atmosphere. The same phenomenon occurs during the second half-period, where the surrounding gas enters into the low pressure region underneath the microplate. This significant change of mass underneath the microplate is reflected through the fourth, eighth, and ninth coefficients that represent the inertia terms that dominate for the simulations with an appreciable displacement of the microplate (small St) and a relatively low oscillating frequency (no gas entrapment) with high speed (high Re), where an appreciable amount of the squeezed gas beneath the microplate flows to the outside (during the first half-period) or *vice versa* (during the second half-period), leading to a substantial change in the fluid's inertia due to the change of mass of the squeezed fluid film (C_4, C_8, and C_9 are $f(\mathrm{ReSt})$). As the frequency further decreases (50 MHz), the change of pressure beneath the microplate decreases, thus decreasing the mass flow rate throughout the film gap thickness region. For this reason, the fourth, eighth, and ninth coefficients peak at the 111.11 MHz case where the microplate's motion, during the first half- period, is fast enough to compress the fluid underneath and slow enough to allow time for this compressed gas to flow outside the gap region (inverse flow direction during the second half- period). The fifth coefficient reflects the compressibility of the squeezed gas as it shows up for the cases of low St, where the microplate displaces an appreciable distance of the film gap (50% in this case).

8 Conclusion

This work presents a combined analytical/numerical technique to develop a new force model for the squeezed film damping force in the vicinity of oscillating microstructures. For the analytical approach, an inviscid and incompressible problem is solved to stress the effect of the inertia on the fluid damping force and, therefore, new terms that reflect the contribution of inertia which are neglected in the classical Reynolds lubrication equation have been formulated. In addition, the DSMC method has been implemented to numerically correct for the proposed model (i.e., to include the viscous and compressibility effects) and, therefore, a more comprehensive damping force model was proposed. The coefficients of the proposed model were plotted to show their dependence on the set of the dimensionless groups governing the fluid behavior.

Acknowledgment

This work was supported, in part, by Dar Al-Handasah.

Nomenclature

b = microplate width
c = damping constant
DSMC = direct simulation Monte Carlo
f = oscillation frequency
F_{net} = net force
h_0 = initial gap film thickness
$h(t)$ = instantaneous gap film thickness
$\dot{h}(t)$ = instantaneous microplate speed
Kn = Knudsen number
L = microplate length
Ma = Mach number
p_a = ambient pressure
p_b = microplate's back face pressure
p_f = microplate's front face pressure
R = radial distance from microplate
Re = Reynolds number
St = Strouhal number
t = microplate thickness
u = horizontal velocity flow field
U = average horizontal velocity flow field
v = vertical velocity flow field
V_a = microplate velocity amplitude
$z(t)$ = instantaneous microplate displacement
δ = oscillation amplitude
μ = dynamic viscosity
ρ = gas density
σ_L, σ_b = squeeze numbers
ω_c = cutoff frequency

References

[1] Blech, J., 1983, "On Isothermal Squeeze Films," J. Lubr. Technol., **105**, pp. 615–620.
[2] Andrews, M., Harm, I., and Turner, G., 1993, "A Comparison of Squeeze-Film Theory With Measurements on a Microstructure," Sens. Actuators, A, **36**, pp. 79–87.
[3] Zook, J., Bums, D., Guckel, H., Snlegowski, J., Engelstad, R., and Feng, Z., 1992, "Characteristics of Polysilicon Resonant Microbeams," Sens. Actuators, A, **35**, pp. 51– 59.
[4] Christian, R., 1966, "The Theory of Oscillating-Vane Vacuum Gauges," Vacuum, **16**, pp. 175–178.
[5] Newell, W., 1968, "Miniaturization of Tuning Forks," Science, **161**, pp. 1320–1326.
[6] Hutcherson, S. and Ye, W., 2004, "On the Squeeze-Film Damping of Micro-Resonators in the Free-Molecule Regime," J. Micromech. Microeng., **14**, pp. 1726–1733.
[7] Bao, M., Yang, H., Yin, H., and Sun, Y., 2002, "Energy Transfer Model for Squeeze-Film Air Damping in Low Vacuum," J. Micromech. Microeng., **12**, pp. 341–346.
[8] Blom, F., Bouwstra, S., Elwenspoek, M., and Fluitman, J., 1992, "Dependence of the Quality Factor of Micromachined Silicon Beam Resonators on Pressure and Geometry," J. Vac. Sci. Technol. B, **10**(1), pp. 19–26.
[9] Li, P. and Fang, Y., 2010, "A Molecular Dynamics Simulation Approach for the Squeeze-Film Damping of MEMS Devices in the Free Molecular Regime," J. Micromech. Microeng., **20**, p. 035005.
[10] Bao, M., Sun, Y., Zhou, J., and Huang, Y., 2006, "Squeeze-Film Air Damping of a Torsion Mirror at a Finite Tilting Angle," J. Micromech. Microeng., **16**, pp. 2330–2335.
[11] Langlois, W. E., 1962, "Isothermal Squeeze Films," Q. Appl. Math., **20**, pp. 131–150.
[12] Starr, J. B., 1990, "Squeeze-Film Damping in Solid-State Accelerometers," Technical Digest IEEE Solid State Sensor and Actuator Workshop, Hilton Head Island, SC, pp. 44–47.
[13] Veijola, T., Tinttunen, T., Nieminen, H., Ermolov, V., and Ryhnen, T., 2002, "Gas Damping Model for an RF MEM Switch and Its Dynamic Characteristics," Proceedings of International Microwave Symposium (IMS), Seattle, WA, pp. 1213–1216.
[14] Li, P., Hu, R., and Fang, Y., 2007, "A New Model for Squeeze-Film Damping of Electrically Actuated Microbeams Under the Effect of a Static Deflection," J. Micromech. Microeng., **17**, pp. 1242–1251.
[15] Younis, M. and Nayfeh, A., 2007. "Simulation of Squeeze-Film Damping of Microplates Actuated by Large Electrostatic Load," ASME J Comput. Nonlinear Dyn., **2**, pp. 232–241.
[16] Sumali, H., 2007, "Squeeze-Film Damping in the Free Molecular Regime: Model Validation and Measurement on a MEMS," J. Micromech. Microeng., **17**, pp. 2231–2240.
[17] Mol, L., Rocha, L., Cretu, E., and Wolffenbuttel, R., 2009, "Squeezed Film Damping Measurements on a Parallel-Plate MEMS in the Free Molecule Regime," J. Micromech. Microeng., **19**, p. 074021.
[18] Zhang, B. and Fang, D., 2009, "Modeling and Modification of the Parallel Plate Variable Mems Capacitors Considering Deformation Issue," Mech. Mach. Theory, **44**, pp. 647–655.
[19] Niessner, M., Schrag, G., Wachutka, G., Iannacci, J., Reutter, T., and Mulatz, H., 2009), "Non-Linear Model for the Simulation of Viscously Damped RF-MEMS Switches at Varying Ambient Pressure Conditions," Proceedings of the Eurosensors XXIII Conference, Procedia Chem. **1**, pp. 618–621.

Downloaded from http://asmedigitalcollection.asme.org/tribology/article-pdf/136/2/021705/6284892/trib_136_02_021705.pdf by American University of Beirut Aub user on 20 March 2024

[20] Sumali, H. and Carne, T., 2008, "Air Damping on Micro-Cantilever Beams," Proceedings of the International Modal Analysis Conference.
[21] Hosaka, H., Itao, K., and Kuroda, S., 1995, "Damping Characteristics of Beam-Shaped Micro-Oscillators," Sens. Actuators, A, **49**, pp. 87–95.
[22] Kokubun, K., Hirata, M., Murakami, H., Toda, Y., and Ono, M., 1984, "A Bending and Stretching Mode Crystal Oscillator as a Friction Vacuum Gauge," Vacuum, **34**, pp. 731–735.
[23] Veijola, T., 2004, "Compact Models for Squeezed-Film Dampers With Inertial and Rarefied Gas Effects," J. Micromech. Microeng., **14**, pp. 1109–1118.
[24] Gallis, M. and Torczynski, J., 2004, "An Improved Reynolds-Equation Model for Gas Damping of Microbeam Motion," J. Microelectromech. Syst., **13**(4), pp. 653–659.
[25] Lee, J., Tung, R., Raman, A., Sumali, H., and Sullivan, J., 2009, "Squeeze-Film Damping of Flexible Microcantilevers at Low Ambient Pressures: Theory and Experiment," J. Micromech. Microeng., **19**, p. 105029.
[26] Guo, X. and Alexeenko, A., 2009, "Compact Model of Squeeze-Film Damping Based on Rarefied Flow Simulations," J. Micromech. Microeng., **19**, p. 045026.
[27] Diab, N. and Lakkis, I., 2012, "DSMC Simulations of Squeeze Film Between a Micro Beam Undergoing Large Amplitude Oscillations and a Substrate," Proceedings of the ASME 2012 10th International Conference on Nanochannels, Microchannels, and Minichannels (ICNMM), Puerto Rico.
[28] Diab, N. and Lakkis, I., 2012, "DSMC Simulations of Squeeze Film Under a Harmonically Oscillating Micro RF Switch With Large Tip Displacements," Proceedings of the ASME 2012 International Mechanical Engineering Congress and Exposition, Houston, TX.
[29] Griffin, W. S., Richardson, H. H., and Yamanami, S., 1966, "A Study of Fluid Squeeze-Film Damping," ASME, J. Basic Eng., 88(2), pp. 451–456.
[30] Senturia, S., 2004, *Microsystem Design*, Springer, New York.

Downloaded from http://asmedigitalcollection.asme.org/tribology/article-pdf/136/2/021705/6284892/trib_136_02_021705.pdf by American University of Beirut Aub user on 20 March 2024